SUPPORTING INFORMATION

Formation of Uniform Porous Yolk-Shelled $MnCo_2O_4$ Microrugbys with Enhanced Electrochemical Performance for Lithium Storage and Oxygen Evolution Reaction

Jia Li[a], Yongxing Zhang[a,*], Li Li[a], Yanming Wang[a], Lei Zhang[a], Baojie Zhang[a], Fei Wang [a], Bing Li[a] and Xin-Yao Yu[b,c,*]

[a]Key Laboratory of Green and Precise Synthetic Chemistry and Application, Ministry of Education, Huaibei Normal University, Huaibei 235000, P. R. China.

[b]Institutes of Physical Science and Information Technology, Anhui University, Hefei 230601, P. R. China

[c]School of Materials Science & Engineering, Zhejiang University, Hangzhou 310027, P. R. China

[a,*]Corresponding author: zyx07157@mail.ustc.edu.cn;

[b, c, *]Corresponding author: yuxinyao@ahu.edu.cn

Experimental Section

Materials Synthesis. In a typical synthesis, 0.5 mmol of $Mn(CH_3COO)_2 \cdot 4H_2O$, 1 mmol of $Co(CH_3COO)_2 \cdot 4H_2O$, and 16 mmol of urea were added into a mixed solution of 15 mL deionized water and 15 mL glycerol and stirred at room temperature for 15 mins. Then 1 mmol of STAB was added and kept stirring at room temperature for another 15 mins to form a transparent solution. The resulting solution was transferred into a 50 mL Teflon-lined stainless autoclave and kept at 140 °C for 10 h. After cooling to room temperature, the pink precursor was collected and washed with deionized water and ethanol for several times, and dried in a vacuum oven at 60 °C for 12 h. Then, the as-prepared product was annealed at 600 °C in air for 10 h with a temperature ramp rate of 3 °C/min to obtain porous yolk-shelled $MnCo_2O_4$ microrugbys (YSM-MCO). The pink precursor was finally converted into the black powder. For comparison, $MnCo_2O_4$ with twin notched morphologies (denoted as TN-MCO) were prepared through a similar procedure without adding STAB. The Co_3O_4 microcubes were synthesized under the same condition except that only $Co(CH_3COO)_2 \cdot 4H_2O$ was used instead of the mixture of $Co(CH_3COO)_2 \cdot 4H_2O$ and $Mn(CH_3COO)_2 \cdot 4H_2O$. The Mn_2O_3 twin notched spheres were synthesized under the same condition except that only $Mn(CH_3COO)_2 \cdot 4H_2O$ was used instead of the mixture of $Co(CH_3COO)_2 \cdot 4H_2O$ and $Mn(CH_3COO)_2 \cdot 4H_2O$.

Materials Characterization. X-ray diffraction (XRD) patterns were obtained in the 2θ range of 10-80° using a Philips X'Pert Pro X-ray diffractometer with Cu Kα radiation (1.5418 Å). Field emission scanning electron microscopy (FESEM) images were taken on a FESEM (Quanta 200 FEG)) operated at an accelerating voltage of 10.0 kV. Transmission electron microscopy (TEM) and high resolution transmission electron microscope (HRTEM) images were obtained on a JEOL

JEM-2010 transmission electron microscope, equipped with X-ray energy dispersive spectroscopy (EDS) capabilities working at an acceleration voltage of 200 kV. Thermogravimetric analysis was conducted on a TGA-2050 (TA Corp.) thermal analysis system under a heating rate of 5 °C/min from 20 to 800 °C with an air flow rate of 100 mL/min. Surface analysis of the samples was performed using X-ray photoelectronic spectrometer (VGESCA-LABMKII, XPS). The nitrogen adsorption-desorption isotherms and pore-size distributions of the as-synthesized samples were measured by Brunauer-Emmett-Teller (BET) and Barrett-Joyner-Halenda (BJH) methods (Micrometrics, ASAP2020M + C).

Lithium Storage Performance Measurement. The electrochemical performances of the as-synthesized samples were tested by CR2016-type coin cells with high-purity lithium foil as the counter/reference electrode. The working electrodes were prepared by blending 70 wt% active material, 20 wt% Super P conductive carbon, and 10 wt% polyvinylidene difluoride binder onto copper foil. The electrode sheets with a diameter of 12 mm were punched out and dried at 80 °C for 12 h in a vacuum oven. The loading amount of active material: ~1 mg cm^{-2}. The Celgard 2400 membrane was used as the separator. The test electrolyte solution was formed by dissolving 1 M $LiPF_6$ in a mixture solvent of ethylene carbonate (EC), ethyl methyl carbonate (EMC) and dimethyl carbonate (DMC) (EC: EMC: DMC = 1: 1: 1, in volume ratio). The galvanostatic charging/discharging cycles were measured by a LAND CT2001 cell tester between 0.01 and 3.0 V at 25 °C. Cyclic voltammetry (CV, 0.1 mV/s) and electrochemical impedance spectroscopy (EIS, 0.01-100 kHz) measurements were both evaluated by a CHI760E electrochemical workstation. The diffusion coefficient (D) of Li-ions is calculated by utilized the Eqs. 1–3:

$$\omega = 2\pi f \quad (1)$$

$$Z' = R + \sigma\omega^{-1/2} \quad (2)$$

$D = 0.5R^2T^2/A^2n^4F^4C^2\sigma^2$ (3)

where R is the gas constant, f is the frequency, σ is the Warburg coefficient, T is Kelvin temperature, A is the contact area of electrodes, n is the electronic transfer number per molecule during the intercalation, F is the Faraday constant and C is the molar concentration of Li-ions. In order to test the electronic conductivity of active material bonded to copper foil, we replaced the lithium sheet of counter electrode with copper foil (denoted as Cu/active material/Cu). The electronic conductivities of YSM-MCO and TN-MCO on the Cu/YSM-MCO/Cu and Cu/TN-MCO/Cu were measured by applying a 0.1 V direct current (DC)/Cu cells.

OER Performance Measurement. Electrocatalyst powder (5 mg) was dispersed in a mixture of 0.6 mL of water and 0.4 mL of ethanol with 30 μL of Nafion solution, and then the mixture was under continuously mixed ultrasonically for 0.5 h to obtain a homogenous ink. For the fabrication of working electrodes, the YSM-MCO were deposited on nickel (Ni) foam (NF). In a typical experiment, the NF (about 1 cm × 2 cm) was cleaned using 3 M hydrochloric acid solution for 5 min in an ultrasound bath. Then, the NFs were alternately washed with deionized water and ethanol for 10 min. The catalyst ink (10 μL) was sucked, released (10 times) and then dropped on the NF by using a pipette (loading amount: ~0.5 mg cm^{-2}). 1 M potassium hydroxide (KOH) solution was used as the electrolyte. A silver/silver chloride (Ag/AgCl) electrode and platinum sheet were used as the reference and the counter electrodes, respectively. The linear sweep voltammetry (LSV) was measured from 0 to 0.8 V with a sweep rate of 5 mV s^{-1}. All polarization curves were corrected with *iR*-compensation. The electrochemical impedance spectroscopy (EIS) measurements were carried out at open circuit potential, and the frequency scan range was from 1000 kHz to 0.01 Hz. The pH value of the 1 M KOH was ~14. The potentials were converted to values referred to the reversible hydrogen electrode (RHE) using the formula: $E_{RHE} = E_{Ag/AgCl} + 0.197 + 0.059 \times pH$,

where $E_{Ag/AgCl}$ is the experimentally measured potential against the Ag/AgCl reference electrode. The overpotential (η) was calculated using the following equation: $\eta = E_{RHE} - 1.23$. The Tafel plots are derived from the polarization curves via the Tafel equation ($\eta = b \times \log j + a$, where η is the overpotential, j is the current density, and b is the Tafel slope).

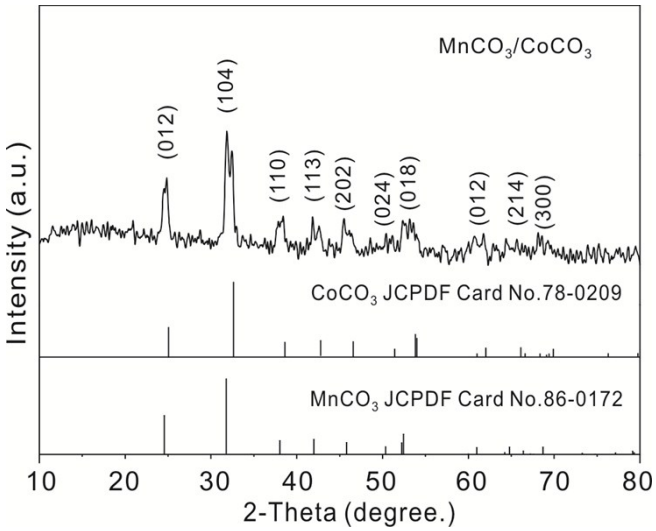

Fig. S1 XRD pattern of the $MnCO_3/CoCO_3$ microrugby precursor

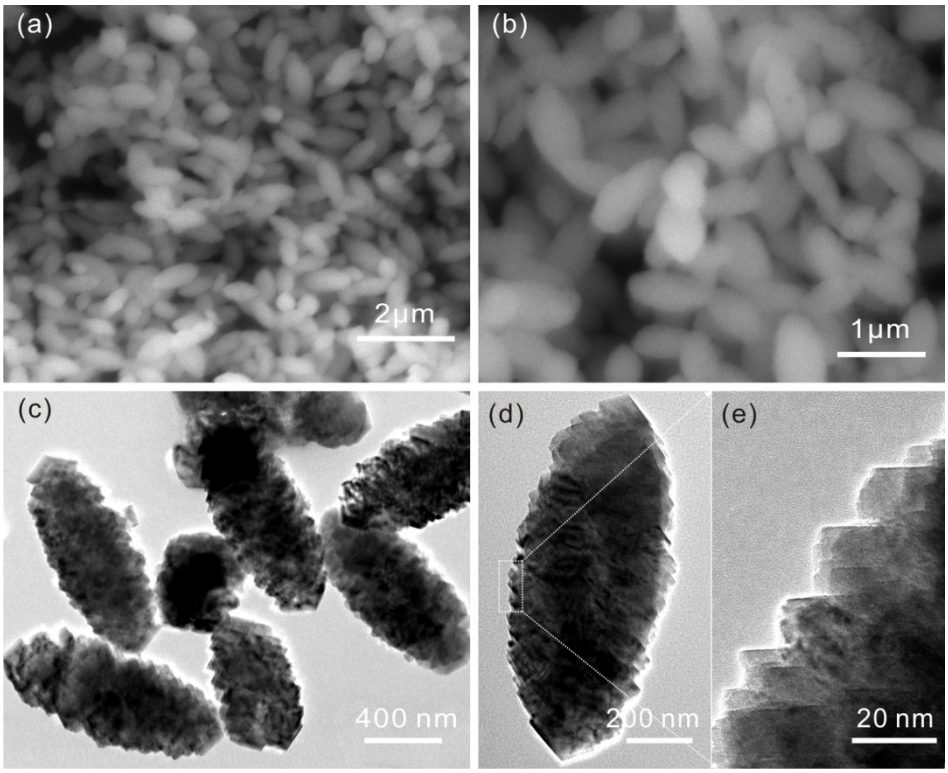

Fig. S2 (a,b) SEM and (c-e) TEM images of the $MnCO_3/CoCO_3$ microrugby precursor

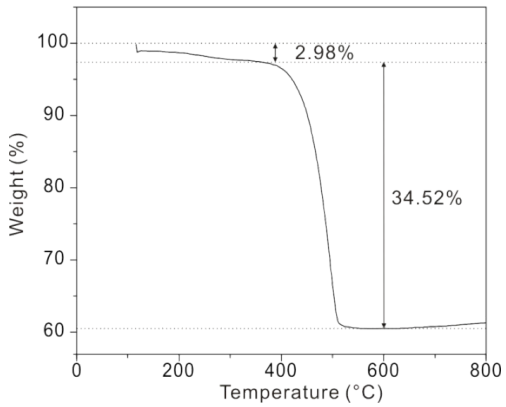

Fig. S3 TGA curve of the $MnCO_3/CoCO_3$ microrugby precursor in air with an increasing temperature rate of 5 °C /min. The TGA curve of the $MnCO_3/CoCO_3$ precursor displays two major weight loss steps. The first weight loss (2.98%) below 400 ºC is attributed to the loss of adsorbed water, while the second one (34.52%) is due to the thermal decomposition of $MnCO_3/CoCO_3$ to $MnCo_2O_4$

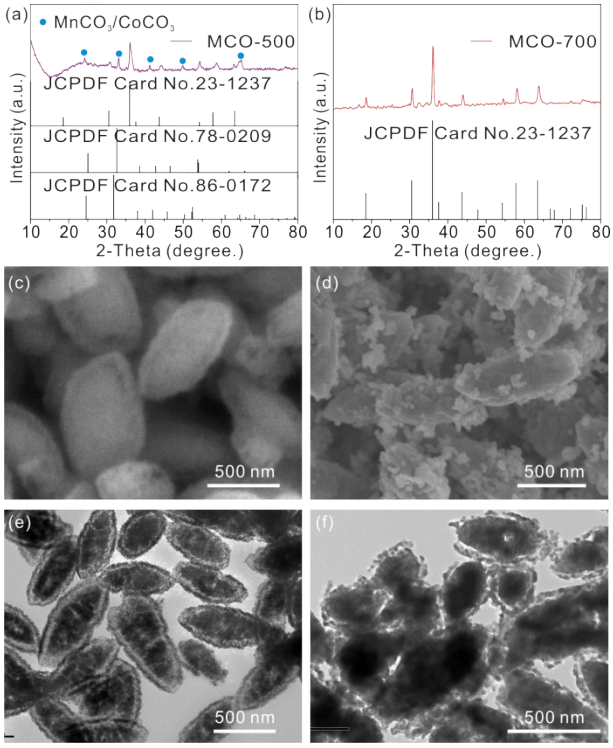

Fig. S4 (a,b) XRD patterns, (c,d) SEM images, and (e,f) TEM images of the products obtained at 500 ^{o}C (denoted as MCO-500) (a,c,e) and 700 ^{o}C (denoted as MCO-700) (b,d,f)

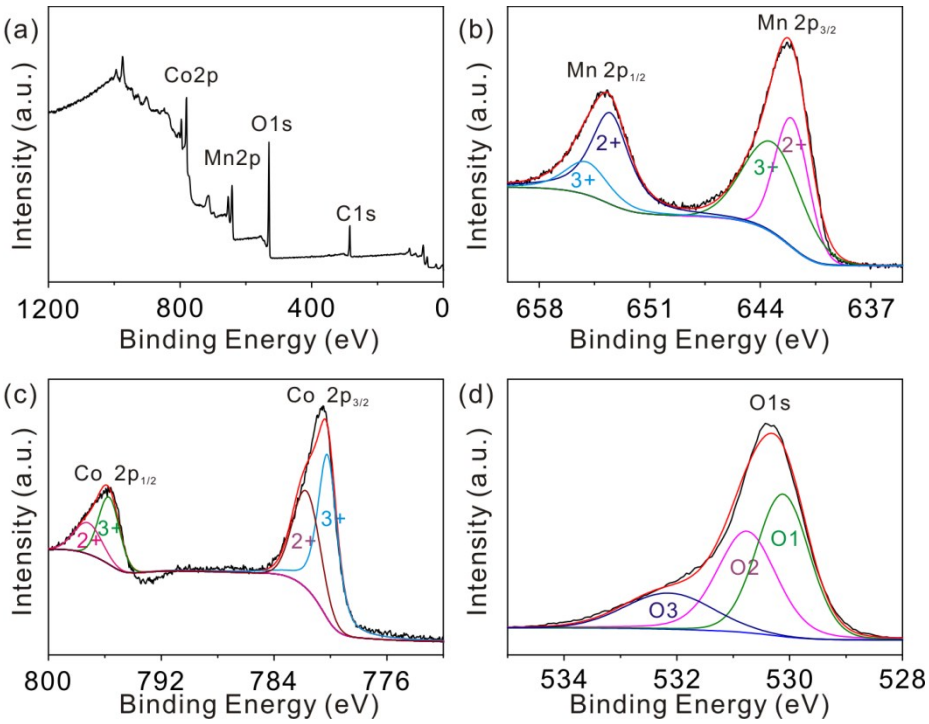

Fig. S5 X-ray photoelectron spectroscopy (XPS) spectra of the YSM-MCO: (a) Survey spectrum and (b-d) high-resolution spectra of Mn 2p (b), Co 2p (c), and O 1s (d)

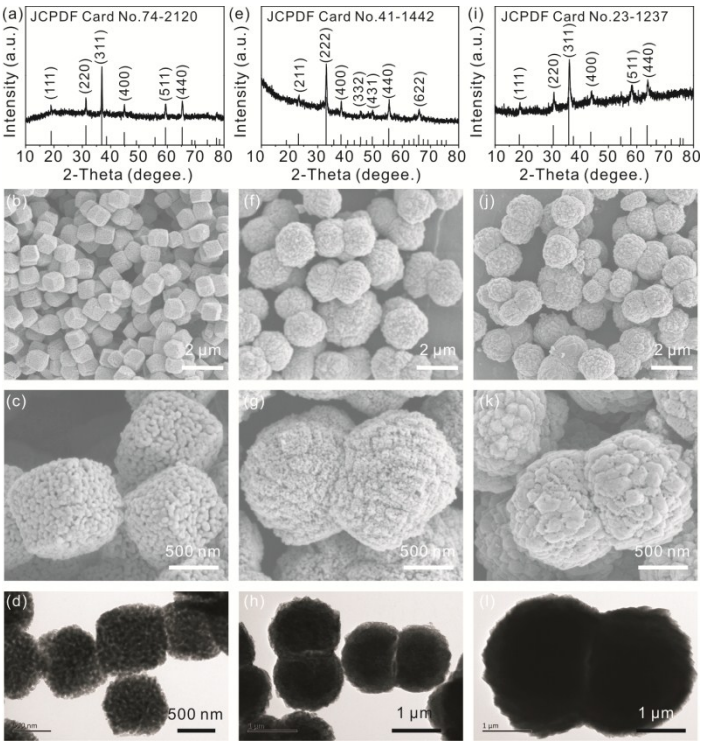

Fig. S6 (a,e,i) XRD patterns, (b,c,f,g,j,k) SEM images, and (d,h,l) TEM images of Co_3O_4 (a-d), Mn_2O_3 (e-h), and TN-MCO (i-l)

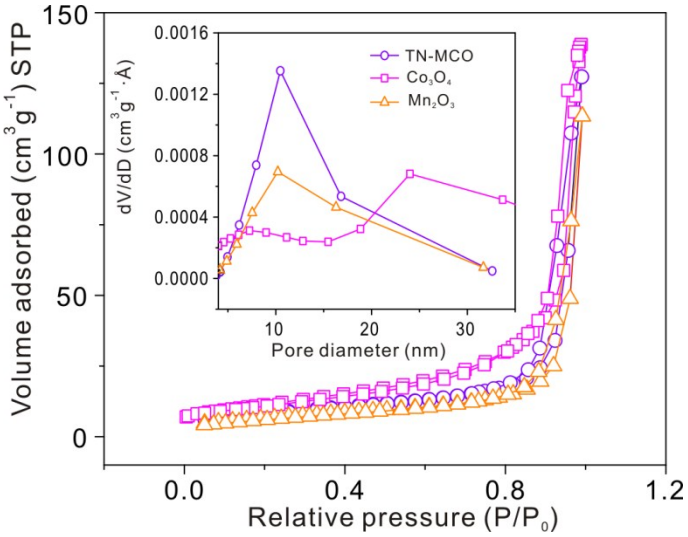

Fig. S7 Typical nitrogen gas adsorption-desorption isotherms and pore-size distribution curves (inset) of Co_3O_4, Mn_2O_3, and TN-MCO

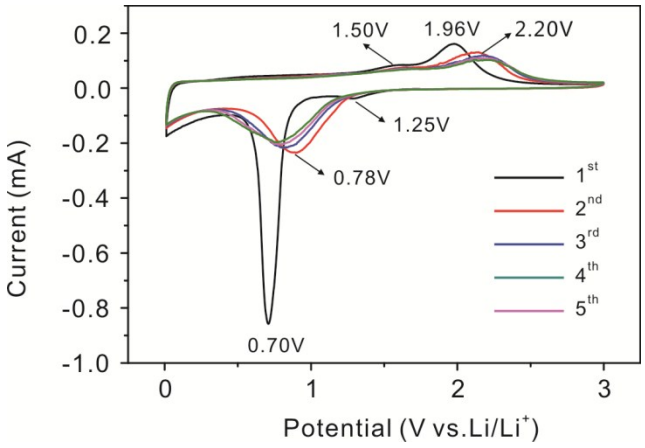

Fig. S8 CV curves for the initial five cycles at a scan rate of 0.1 mV s^{-1} in the voltage range of 0.01-3.0 V

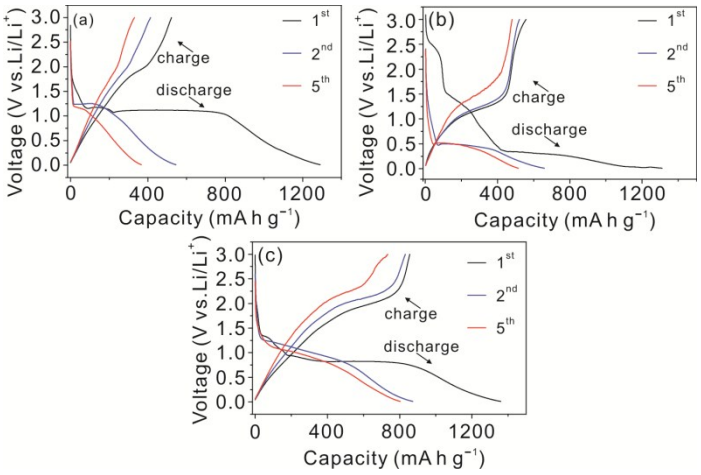

Fig. S9 Galvanostatic discharge-charge curves of (a) Co_3O_4, (b) Mn_2O_3, and (c) TN-MCO for the 1st, 2nd, and 5th cycles at the current density of 0.1 A g^{-1}

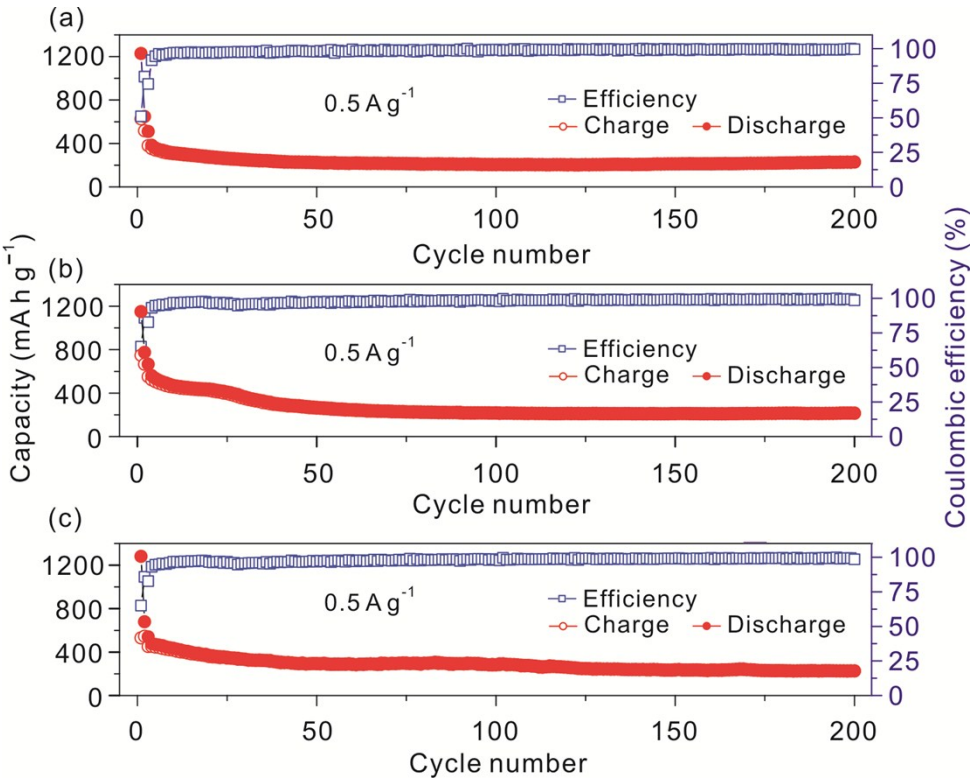

Fig. S10 Cycling performances of (a) Co_3O_4, (b) Mn_2O_3, and (c) TN-MCO in Li half cells at 0.5 A g^{-1} for 200 cycles

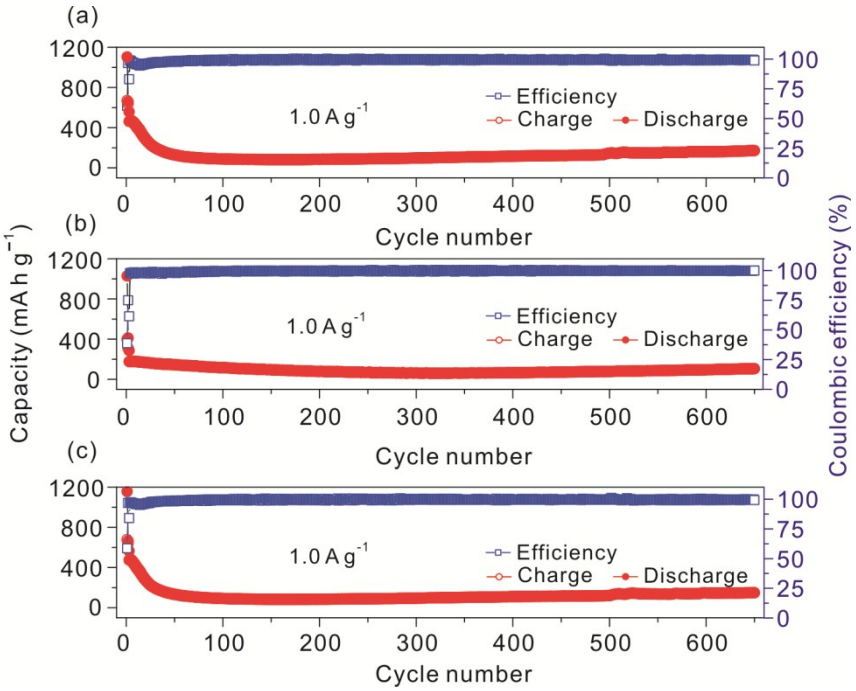

Fig. S11 Long cycling performances of (a) Co_3O_4, (b) Mn_2O_3, and (c) TN-MCO in Li half cells at 1 A g^{-1} for 650 cycles

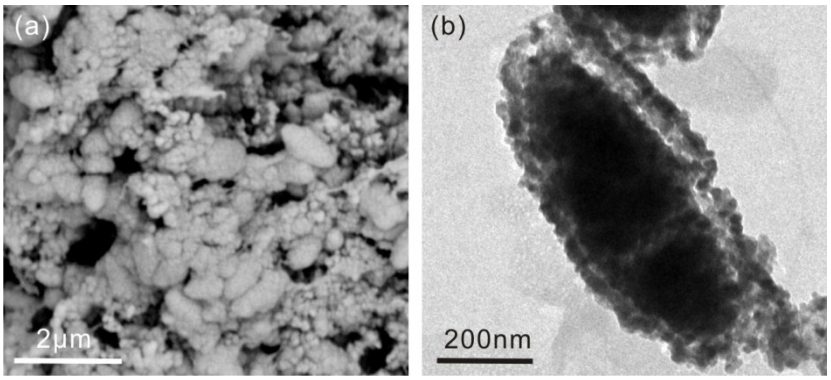

Fig. S12 (a) SEM and (b) TEM images of the YSM-MCO electrode for LIBs after 650 cycles

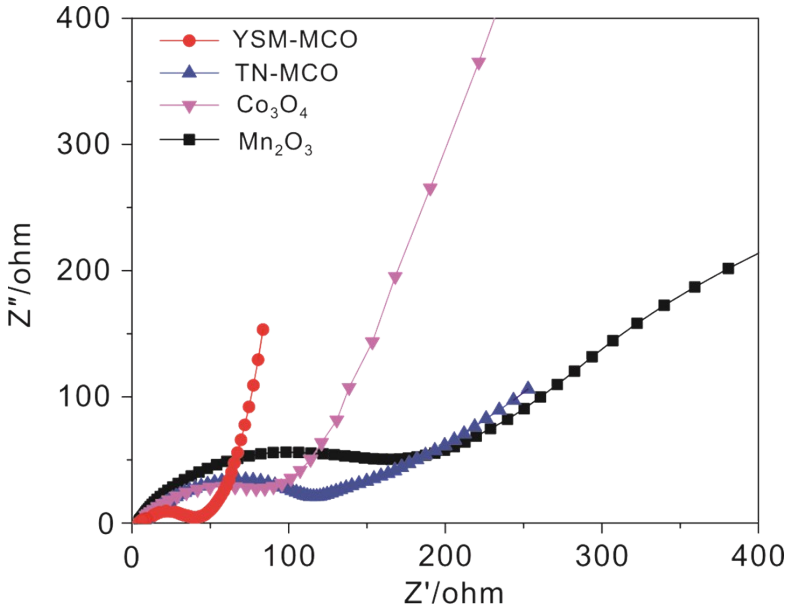

Fig. S13 Electrochemical impedance spectra of the YSM-MCO (red circles), Co_3O_4 (purple circles), Mn_2O_3 (black squares), and TN-MCO (blue triangles) electrodes after 150 charge-discharge cycles at 0.5 A g^{-1}

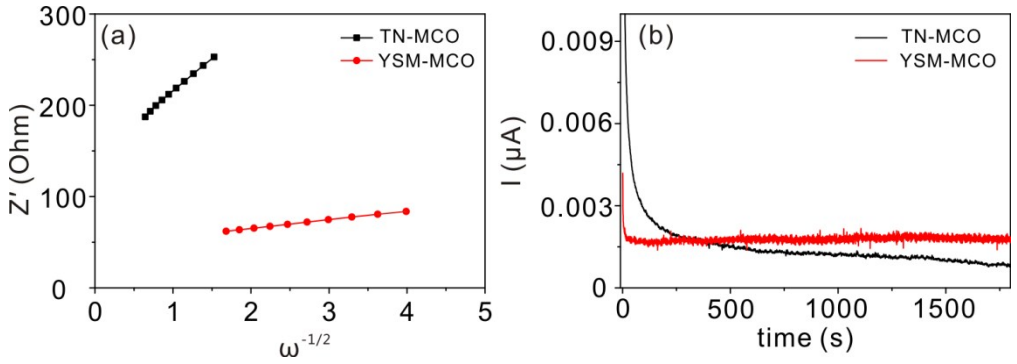

Fig. S14 (a) Relationship Z' and $\omega^{-1/2}$ at low frequency of YSM-MCO and TN-MCO; (b) Current-time curves of Cu/YSM-MCO/Cu and Cu/TN-MCO/Cu

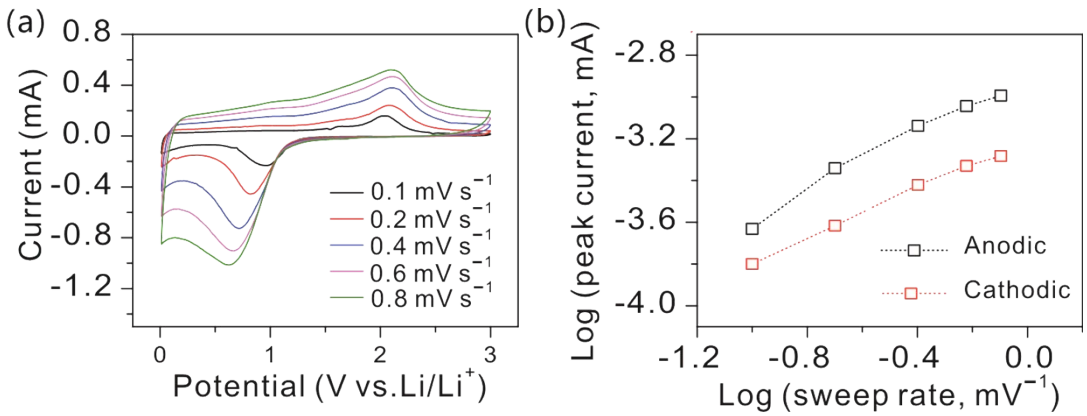

Fig. S15 (a) CV curves of the YSM-MCO electrode at different scan rates. (b) log *i* vs.log *v* plots at oxidation and reduction states

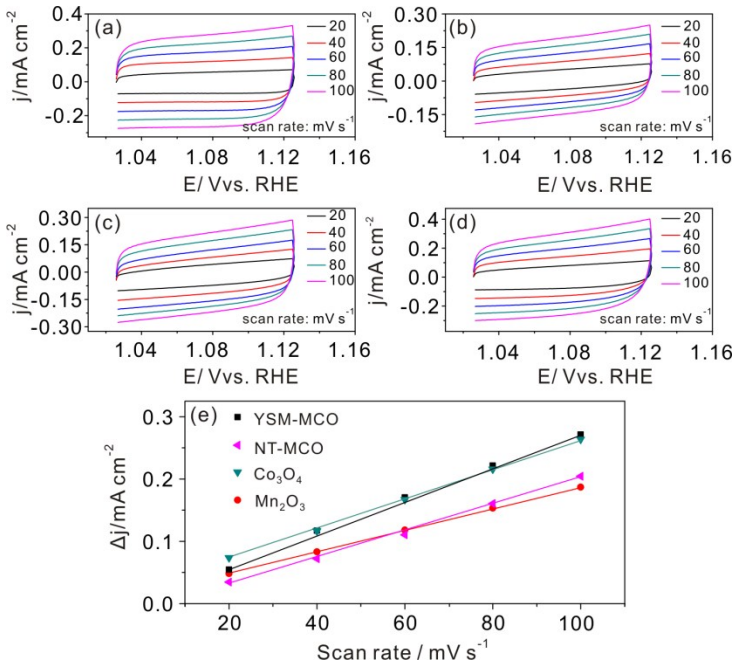

Fig. S16 CV curves at different scan rates for the (a) YSM-MCO, (b) Mn_2O_3, (c) TN-MCO, and (d) Co_3O_4 electrodes. (e) Current density ($\Delta j = j_a - j_c$) as a function of scan rate derived from (a-d) for the four catalysts

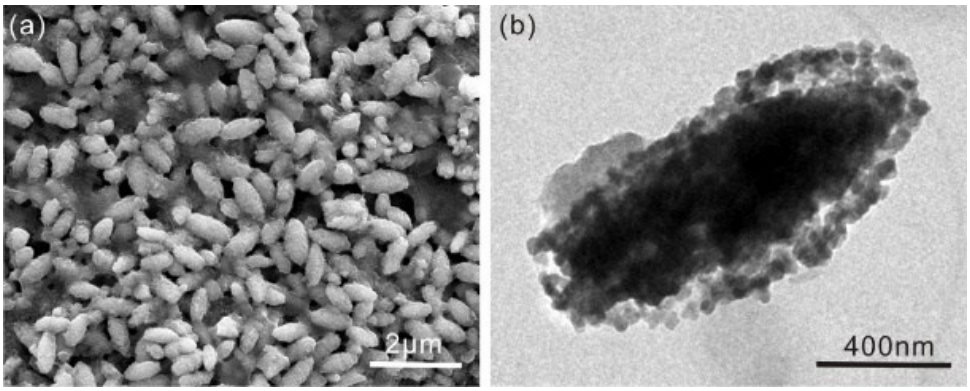

Fig. S17 (a) SEM and (b) TEM image of the YSM-MCO electrode after OER test for 80 h

Table S1 Comparison of lithium storage properties of $MnCo_2O_4$-based anodes

Anodes	Capacity (mAh g^{-1})/cycle number	Current density (mA g^{-1})	Ref.
$MnCo_2O_4$ quasi-hollow spheres	610/100th	400	1
$MnCo_2O_4$ nanoparticles	584.3/250th	2000	2
Flake-like $MnCo_2O_4$	952/100th	100	3
Diamond-like $MnCo_2O_4$	720.4/200th	300	4
Core-shelled $MnCo_2O_4$ ellipsoidal	620/50th	400	5
Multiporous core-shelled $MnCo_2O_4$	700/50th	400	6
$MnCo_2O_4$ nanowire	895.8/50th	100	7
Erythrocyte-like $MnCo_2O_4$	960/100th	200	8
Porous yolk-shelled $MnCo_2O_4$ microrugbys	**742.2/200th** **475.4/650th**	**500** **1000**	**This work**

Table S2 Summary of the OER catalytic activity of different $MnCo_2O_4$-based electrocatalysts

Catalyst materials	overpotential at10 mA cm^{-2} (V)	Ref.
Porous yolk-shelled $MnCo_2O_4$ microrugbys	**0.36**	**This work**
Nano-$MnCo_2O_{4.5}$	0.41	9
$MnCo_2O_4$ nanofibers	0.45	10
$MnCo_2O_4$ microspheres	0.49	11
$MnCo_2O_4$ nanoparticles	0.49	12
$Mn_xCo_{3-x}O_4$ nanocrystals	0.47	13

Table S3 The Li^+ diffusion coefficient and electron conductivity of YSM-MCO and TN-MCO, respectively

Materials	Li^+ diffusion coefficient (cm^2/s)	Electron conductivity (S/cm)
YSM-MCO	1.24×10^{-11}	6×10^{-11}
TN-MCO	1.6×10^{-12}	2.85×10^{-12}

References

1. J. Li, S. Xiong, X. Li and Y. Qian, *Nanoscale*, 2013, **5**, 2045-2054.
2. C. Chen, B. R. Liu, Q. Ru, S. M. Ma, B. N. An, X. H. Hou and S. J. Hu, *J. Power Sources*, 2016, **326**, 252-263.
3. A. K. Mondal, D. Su, S. Chen, A. Ung, H. S. Kim and G. Wang, *Chem. Eur. J.*, 2015, **21**, 1526-1532.

4. L. L. Zhang, Q. L. Tang, X. H. Chen, B. B. Fan, K. K. Xiao, S. Y. Zhang, W. N. Deng and A. P. Hu, *J. Alloys Compd.*, 2017, **722**, 387-393.

5. G. Huang, S. Xu, Z. Xu, H. Sun and L. Li, *ACS Appl. Mater. Interfaces*, 2014, **6**, 21325-21334.

6. X. Wu, S. Li, B. Wang, J. Liu and M. Yu, *New J. Chem.*, 2015, **39**, 8416-8423.

7. L. Li, Y. Q. Zhang, X. Y. Liu, S. J. Shi, X. Y. Zhao, H. Zhang, X. Ge, G. F. Cai, C. D. Gu, X. L. Wang and J. P. Tu, *Electrochim. Acta*, 2014, **116**, 467-474.

8. G. H. Li, Q. H. Zhai, Q. Liu and R. C. Jin, *Cryst. Res. Technol.*, 2017, **52**, 1600255.

9. Z. Y. Bai, J. M. Heng, Q. Zhang, L. Yang and F. F. Chang, *Adv. Energy Mater.*, 2018, **8**, 1802390.

10. K. N. Jung, S. M. Hwang, M. S. Park, K. J. Kim, J. G. Kim, S. X. Dou, J. H. Kim and J. W. Lee, *Sci Rep.*, 2015, **5**, 7665.

11. P. W. Menezes, A. Indra, N. R. Sahraie, A. Bergmann, P. Strasser and M. Driess, *ChemSusChem*, 2015, **8**, 164-171.

12. C. H. Xu, M. H. Lu, Y. Zhan and J. Y. Lee, *RSC Adv.*, 2014, **4**, 25089-25092.

13. T. Zhao, S. Gadipelli, G. He, M. J. Ward, D. Do, P. Zhang and Z. Guo, *ChemSusChem*, 2018, **11**, 1295-1304.